Materials Science
ISSN: 0974-7486

Materials Science: An Indian Journal

Commentary | Vol 14 Iss 13

Study the Effect of Titanium Dioxide on Microstructure, Electrochemical Corrosion Parameters, Thermal Behavior and Internal Friction of Hexa Tin-Bismuth Based Alloy

El-Bediwi AB[1*], Bader S[1], and Khalifa F[1,2]

[1]Physics Department, Faculty of Science, Mansoura University, Egypt

[2]Sirte University, Sirte, Libya

[*]**Corresponding author:** Abu Bakr El-Bediwi, Metal Physics Laboratory, Physics Department, Faculty of Science, Mansoura University 35516, Egypt, Tel: + 050 2202266; E-mail: baker_elbediwi@yahoo.com

Received: October 07, 2016; **Accepted:** November 10, 2016; **Published:** November 30, 2016

Abstract

Effect of adding titanium dioxide nanoparticle (TiO_2) on microstructure, thermal parameters, internal friction, and electrochemical corrosion behaviour of $Sn_{61}Bi_{25}Sb_5Zn_4Al_3Ag_2$ alloy has been studied using different experimental techniques. Microstructure of $Sn_{61}Bi_{25}Sb_5Zn_4Al_3Ag_2$ alloy changed after adding TiO_2 nanoparticles. Lattice microstrain of $Sn_{61}Bi_{25}Sb_5Zn_4Al_3Ag_2$ alloy increased after adding TiO_2 nanoparticles. Crystal size of β-Sn phase in $Sn_{61}Bi_{25}Sb_5Zn_4Al_3Ag_2$ alloy varied after adding TiO_2 nanoparticles. $Sn_{61}Bi_{25}Sb_5Zn_4Al_{2.4}Ag_2(TiO_2)_{0.6}$ alloy has higher lattice microstrain and lower β-Sn phase crystal size. Internal friction and thermal diffusivity values of $Sn_{61}Bi_{25}Sb_5Zn_4Al_3Ag_2$ alloy decreased up to 0.9 wt% TiO_2 and then increased with increasing the ratio of TiO_2.

Keywords:* TiO_2 *nanoparticles; Vickers hardness; Corrosion parameters; Internal friction; Hexa tin-bismuth based alloy

Introduction

There are many uses of fusible alloys such as solder alloys in electronics and industry. In industry, alloys contain bismuth in order to lower the melting point. Microstructure, elastic modulus, internal friction, Vickers hardness, electrical resistivity and thermal parameters of $Sn_{80}Sb_{15}Pb_5$ alloy varied after adding Cu or Al or Bi or In metals [1]. Matrix microstructure, corrosion parameters, elastic modulus, internal friction, Vickers hardness, electrical resistivity and thermal parameters of $SnSb_{13}$ alloy changed after adding Cu or Bi or Al or Pb or Zn or Ag elements [2]. Melting point, mechanical properties, contact angle and electrochemical parameters of $Sn_{72}Bi_{24}Zn_4$ alloy varied after adding Cu or In or Al or Se or Ag elements. Adding Cu or Al or Se or Ag improved mechanical and electrical properties of $Sn_{72}Bi_{24}Zn_4$ alloy [3]. Microstructure, electrical, mechanical and thermal properties of $Bi_{58}Sn_{42}$ rapidly solidified alloy have been studied [4]. The results show that, it has good soldering

Citation: El-Bediwi AB, Bader S, Khalifa F. Study the Effect of Titanium Dioxide on Microstructure, Electrochemical Corrosion Parameters, Thermal Behavior and Internal Friction of Hexa Tin- Bismuth Based Alloy. Mater Sci Ind J. 2016;14(13):109.
© 2016 Trade Science Inc.

properties such as low melting point, mechanical properties, adequate wettability and cost. The 58% Bi-42% Sn, 53% Bi-26% Sn-21% Cd,70% In-30% Sn, 50% Sn-50% In and 3% Sn-37% Bi-10% In alloys have homogenous distribution of two or three phases in the microstructure [5]. Thermodynamic properties and phase equilibrium relationship of Sn-Bi-Zn alloys are determined experimentally and theoretically [6]. Effect of structural modification on electrical and mechanical properties of $SnSb_{10}Cu_2X_2$ (X=Pb or Zn or Se or Ag or Cd) alloys have been studied [7]. The electrical resistivity and hardness of $SnSb_{10}$ increased but internal friction, elastic modulus and thermal diffusivity values decreased after adding bismuth content [8]. Creep behavior, elastic modulus and internal friction of $Sn_{86}Sb_{10}Cu_2X_2$ (X=Pb or Ag or Se or Cd-Zn) alloys have been investigated [9]. Structure, electrical resistivity and elastic modulus of $SnSb_7$ and $SnSb_7X$ (X=Cu or Ag or Cu-Ag) alloys have been studied and the $SnSb_7Ag_2Cu_2$ has best bearing properties such as lowest internal friction, cast and adequate elastic modulus [10]. Microstructure and mechanical properties of $SnZn_{8.55}Ag_XA_{l10.45}Ga_{0.5}$(X=0.5 wt% to 3 wt%) lead free solder alloys were studied and the results show, adding Ag decreased the melting point while maintaining the same strength and ductility as the $Sn_{63}Pb_{37}$ solder alloy [11]. $SnZn_9Bi_1Cu_2In_5$ alloy exhibited low melting point (181°C), wetting angle (23°) and higher elastic modulus (59.9 GPa) which it is required for solder applications [12]. Adding small amount of Ag in near-eutectic Bi-Sn alloys improve the tensile ductility by a factor of more than three and reduce the strain-rate [13]. Electrical resistivity and hardness of $SnSb_{10}$ alloy increased but internal friction, elastic modulus and thermal diffusivity values decreased after adding bismuth content [8]. Bi-Sn eutectic alloy has a good soldering property such as low melting point, mechanical properties, adequate wettability and cost [4]. The aim of this work was to study the effect of titanium dioxide on microstructure, electrochemical corrosion behavior, thermal process and internal friction of hexa tin-bismuth based alloy.

Materials and Methods

Bismuth, tin, antimony, zinc, silver, aluminum and titanium dioxide nanoparticles with high purity (more than 99.5%) were melted in a muffle furnace to use in the production ingots from $Sn_{61}Bi_{25}Sb_5Zn_4Al_{3-X}Ag_2(TiO_2)_X$ alloys. Each composition has a weight of 20 g by using the digital milligram scale and the metals were added according to their weight percent (wt%) in the specimen. The resulting ingots were turned and re-melted again to increase the homogeneity. Compositions of these alloys were weighted to an accuracy ±0.001 mg and melted in a porcelain crucible. Long ribbons of ~4 mm width and ~70 µm thickness were prepared by single roller melt spinning technique. The surface velocity of the roller was 31.4 m/s giving a cooling rate of $\sim 3.7 \times 10^5$ K/s. The alloys then cut into convenient shape for the measurements using double knife cuter. Microstructure of $Sn_{61}Bi_{25}Sb_5Zn_4Al3\text{-}xAg_2(TiO_2)_X$ alloys was performed using Shimadzu X-ray diffractometer (Dx-30, Japan) of Cu-Ka radiation with l=1.54056 Å at 45 kV and 35 mA and Ni-filter in the angular range 2q ranging from 0° to 100° in continuous mode with a scan speed 5 degree/min and scanning electron microscope (JEOL JSM-6510LV, Japan). Thermal analysis was obtained using SDT Q600 (V20.9 Build 20) instrument (USA) with heating rate 10 k/min in the temperature range from 50°C to 400°C. The polarization studies were performed using Gamry Potentiostat/Galvanostat with a Gamry framework system based on ESA 300. The internal friction Q-1 was determined using the dynamic resonance method [14-18] by plotting the amplitude of vibration against the frequency of vibration. The thermal diffusivity D_{th} has been derived by Berry and Pritchett [18] from resonance peak.

Results and Discussion

Microstructure

X-ray diffraction analysis: FIG. 1. a), 1.b), 1.c), 1.d), 1.e) and 1.f) show X-ray diffraction patterns of $Sn_{61}Bi_{25}Sb_5Zn_4Al_{3-X}Ag_2(TiO_2)_X$ alloys.

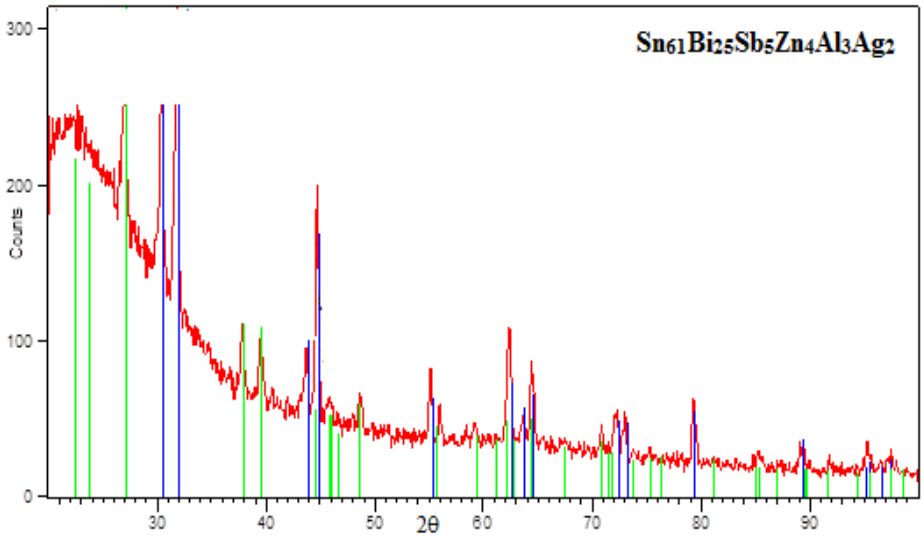

FIG. 1. a) **X-ray diffraction patterns of $Sn_{61}Bi_{25}Sb_5Zn_4Al_3Ag_2$ alloy.**

TABLE 1. a) **X-ray diffraction analysis $Sn_{61}Bi_{25}Sb_5Zn_4Al_3Ag_2$ alloy.**

2θ(°)	d(Å)	Intensity (%)	Peak width-FHWM	Area under peak	Phase	hkℓ
27.0639	3.29477	49.69	0.3149	32.44	Bi	0 1 2
30.3929	2.94106	65.2	0.1968	26.61	Sn	2 0 0
31.8731	2.80777	92.68	0.2165	41.61	Sn	1 0 1
37.8443	2.37736	20.91	0.3149	13.65	Bi	1 0 4
39.5789	2.27708	19.8	0.3149	12.93	Bi	1 1 0
43.7044	2.07122	20.28	0.3149	13.25	Sn	2 2 0
44.7617	2.02473	70.09	0.1968	28.6	Bi	2 1 1
45.7742	1.98227	8.5	0.6298	11.1	Bi	1 1 3
48.6755	1.87068	12.15	0.3149	7.93	Bi	2 0 2
55.164	1.66503	23.79	0.2755	13.59	Sn	3 0 1
55.973	1.64287	10.73	0.3149	7.01	Bi	0 2 4
59.15	1.56198	6.18	0.09	1.17	Bi	1 0 7
62.3292	1.48974	35.73	0.2362	17.5	Sn	1 1 2
64.4473	1.4458	24.8	0.3149	16.2	Sn	3 2 1
70.795	1.33093	7.35	0.4723	7.2	Bi	2 1 4
72.2322	1.30795	13.25	0.4723	12.97	Bi	2 1 4
72.9701	1.29654	13.66	0.3149	8.92	Sn	4 1 1
75.31	1.26196	2.38	0.09	0.45	Sn	4 0 2
79.2066	1.20937	17.26	0.2755	9.86	Sn	3 1 2
85.41	1.1367	3.33	0.09	0.63	Sn	4 3 1
89.2228	1.09774	6.43	0.4723	6.3	Sn	3 1 2
95.3246	1.04295	7.36	0.4723	7.21	Sn	3 3 2
97.3607	1.02565	4.05	1.152	13.07	Sn	5 2 1

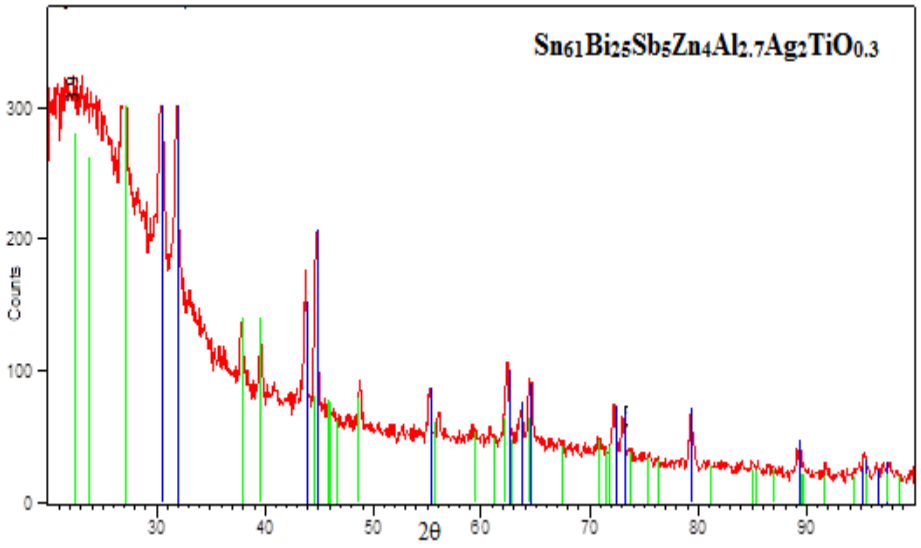

FIG. 1. b) **X-ray diffraction patterns of $Sn_{61}Bi_{25}Sb_5Zn_4Al_{2.7}Ag_2(TiO_2)_{0.3}$ alloy.**

TABLE 1. b) **X-ray diffraction analysis of $Sn_{61}Bi_{25}Sb_5Zn_4Al_{2.7}Ag_2(TiO_2)_{0.3}$ alloy.**

2θ(°)	d(Å)	Intensity (%)	Peak width-FWHM	Area under peak	Phase	hkℓ
22.25	3.99553	71.6	0.001	0.09	Bi	0 0 3
27.1308	3.28681	69.37	0.2362	29.79	Bi	0 1 2
30.5871	2.92282	95.13	0.2165	37.45	Sn	2 0 0
31.9043	2.80509	100	0.2558	46.53	Sn	1 0 1
37.8841	2.37495	25.15	0.3542	16.2	Bi	1 0 4
39.6096	2.27538	25.35	0.3149	14.52	Bi	1 1 0
43.745	2.06939	55.61	0.1968	19.9	Sn	2 2 0
44.8093	2.02268	70.24	0.3936	50.28	Bi	2 1 1
48.7358	1.86851	18.8	0.2362	8.07	Bi	2 0 2
55.1618	1.66509	19.48	0.2755	9.76	Sn	3 0 1
59.45	1.55482	3.25	0.09	0.54	Bi	1 0 7
60.85	1.52236	3.25	0.09	0.54	Sn	1 1 2
62.3612	1.48905	30.87	0.3149	17.68	Sn	1 1 2
64.4852	1.44504	24.83	0.3936	17.77	Sn	3 2 1
70.65	1.33331	4.34	0.09	0.72	Bi	2 1 4
72.2297	1.30799	18.27	0.3149	10.46	Bi	2 1 4
73.0115	1.2959	13.8	0.2362	5.93	Sn	4 1 1
79.3586	1.20744	20.95	0.3936	15	Sn	3 1 2
85.11	1.13994	3.25	0.09	0.54	Sn	4 3 1
89.2914	1.09707	8.7	0.6298	9.97	Sn	3 1 2
95.4629	1.04094	6.59	0.768	12.44	Sn	3 3 2

$Sn_{61}Bi_{25}Sb_5Zn_4Al_3Ag_2$ alloy has line corresponding to β-Sn phase and hexagonal Bi phase which other elements, (Sb, Zn, Al and Ag), dissolved in matrix alloy as shown in FIG. 1a. Also, TiO_2 nanoparticles dissolved in matrix as shown in FIG. 1b)-1f). XRD analysis (2θ(°), d(Å), intensity (%), peak width-FWHM (full width at half maximum), area under peak, phase and Miller indices (hkℓ)) of $Sn_{61}Bi_{25}Sb_5Zn_4Al_{3-X}Ag_2(TiO_2)_X$ alloys listed in TABLES 1a-1f show that, adding TiO_2 nanoparticles caused a change in the feature of formed phases such as peak intensity which is related to crystallinity, peak broadness which is related to crystal size and peak position which is related to orientation. It means TiO_2 nanoparticles dissolved in the alloy

matrix changed its microstructure. Also, the feature around 2θ=30 degree due to formed poly crystal structure even detected or non-detected phases.

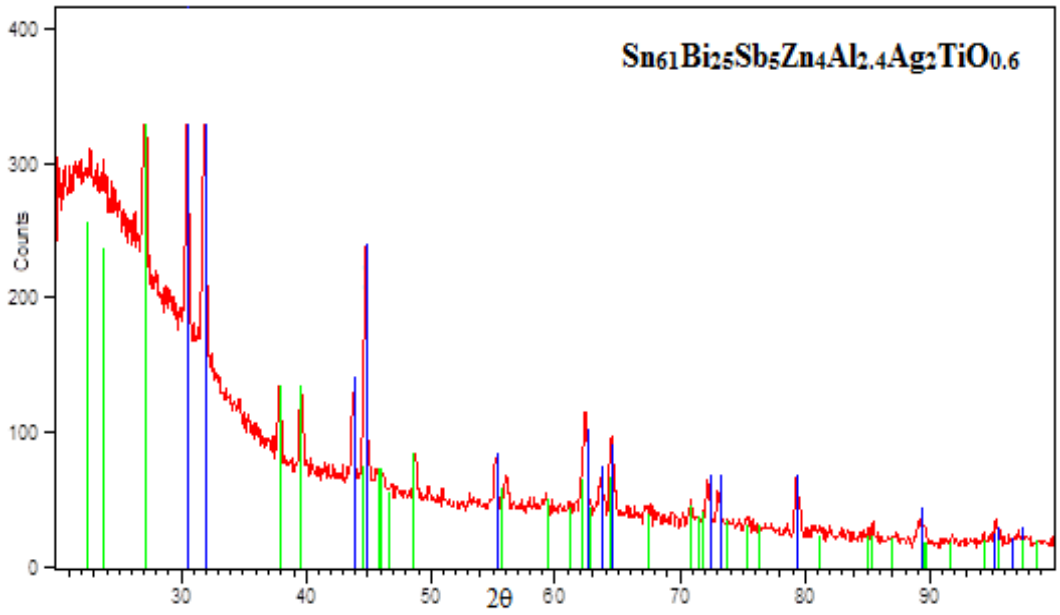

FIG. 1. c) **X-ray diffraction patterns of $Sn_{61}Bi_{25}Sb_5Zn_4Al_{2.4}Ag_2(TiO_2)_{0.6}$ alloy.**

TABLE 1.c) **X-ray diffraction analysis of $Sn_{61}Bi_{25}Sb_5Zn_4Al_{2.4}Ag_2(TiO_2)_{0.6}$ alloy.**

2θ(°)	d(Å)	Intensity (%)	Peak width-FWHM	Area under peak	Phase	hkℓ
27.1656	3.28268	80.17	0.2165	39.6	Bi	0 1 2
30.529	2.92826	86.44	0.2558	50.46	Sn	2 0 0
32.0016	2.79679	100	0.2558	58.38	Sn	1 0 1
37.924	2.37255	22.86	0.3149	16.43	Bi	1 0 4
39.6387	2.27378	27.9	0.2362	15.04	Bi	1 1 0
43.7586	2.06878	27.8	0.1968	12.48	Sn	2 2 0
44.8057	2.02284	75.64	0.2558	44.16	Bi	2 1 1
48.777	1.86703	14.43	0.2755	9.07	Bi	2 0 2
55.1004	1.6668	14.52	0.3936	13.04	Sn	3 0 1
56.0531	1.64071	10.88	0.3936	9.78	Sn	3 0 1
62.4103	1.488	32.34	0.3149	23.23	Sn	1 1 2
64.5262	1.44422	24.12	0.3149	17.33	Sn	3 2 1
72.206	1.30836	11.57	0.3149	8.31	Bi	2 1 4
73.0074	1.29597	8.01	0.3149	5.75	Sn	4 1 1
79.291	1.2083	18.21	0.4723	19.62	Sn	3 1 2
89.2894	1.09709	6.83	0.6298	9.81	Sn	3 1 2
95.4191	1.04131	5.5	0.768	13.02	Sn	3 3 2

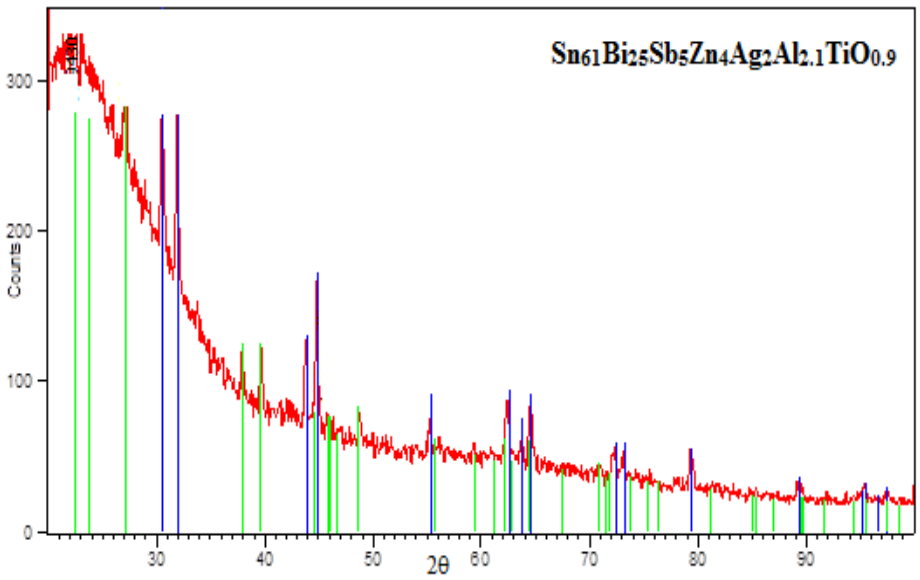

FIG. 1. d) **X-ray diffraction patterns of $Sn_{61}Bi_{25}Sb_5Zn_4Al_{2.1}Ag_2(TiO_2)_{0.9}$ alloy.**

TABLE 1.d) **X-ray diffraction analysis of $Sn_{61}Bi_{25}Sb_5Zn_4Al_{2.1}Ag2(TiO_2)_{0.9}$ alloy.**

2θ(°)	d(Å)	Intensity (%)	Peak width-FWHM	Area under peak	Phase	hkℓ
22.2569	3.9943	94.58	0.1647	13.92	Bi	0 0 3
27.1571	3.28368	59.9	0.2362	18.69	Bi	0 1 2
30.5737	2.92408	90.21	0.1968	23.46	Sn	2 0 0
31.9301	2.80288	100	0.1574	20.81	Sn	1 0 1
37.9348	2.37189	24.86	0.3149	10.35	Bi	1 0 4
39.7244	2.26907	30.97	0.1968	8.06	Bi	1 1 0
43.7591	2.06876	41.85	0.2165	11.97	Sn	2 2 0
44.831	2.02176	71.17	0.1968	18.51	Bi	2 1 1
45.79	1.98162	2.99	0.09	0.36	Bi	1 1 3
48.73	1.86872	14.93	0.09	1.8	Bi	2 1 1
62.377	1.48871	31.39	0.3149	13.06	Sn	1 1 2
64.4966	1.44481	30.64	0.3149	12.75	Sn	3 2 1
70.81	1.33069	6.72	0.09	0.81	Bi	2 1 4
72.21	1.3083	13.44	0.09	1.62	Bi	2 1 4
73.13	1.2941	6.72	0.09	0.81	Sn	4 1 1
79.343	1.20764	20.55	0.3149	8.55	Sn	3 1 2
89.3499	1.0956	7.01	1.152	14.42	Sn	3 1 2
95.21	1.0439	5.23	0.09	0.63	Sn	3 3 2
97.23	1.02753	4.48	0.09	0.54	Sn	5 2 1

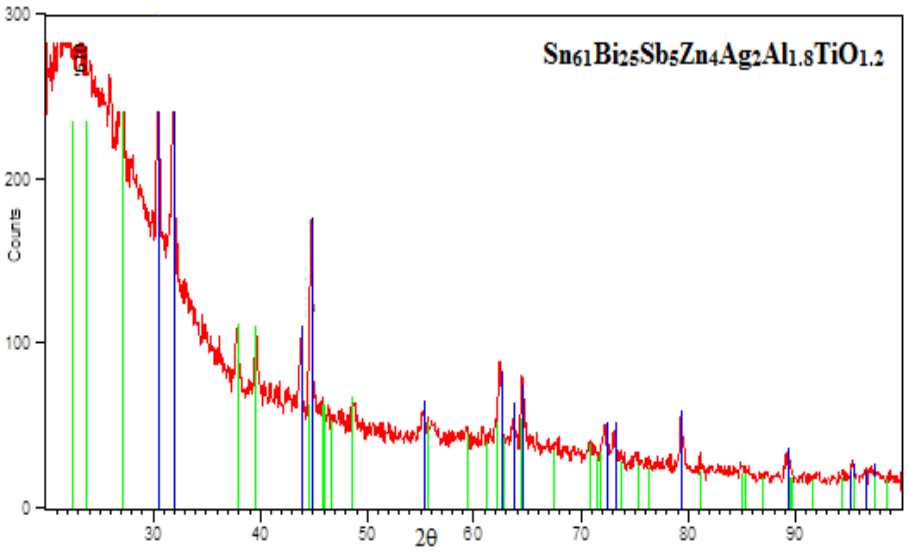

FIG. 1. e) **X-ray diffraction patterns of $Sn_{61}Bi_{25}Sb_5Zn_4Al_{1.8}Ag_2(TiO_2)_{1.2}$ alloy.**

TABLE 1.e) **X-ray diffraction analysis of $Sn_{61}Bi_{25}Sb_5Zn_4Al_{1.8}Ag_2(TiO_2)_{1.2}$ alloy.**

2θ(°)	d(Å)	Intensity (%)	Peak width-FWHM	Area under peak	Phase	h k ℓ
23.2487	3.8261	72.59	0.5327	39.86	Bi	1 0 1
27.1119	3.28905	57.72	0.2362	20.79	Bi	0 1 2
30.5608	2.92528	56.42	0.3542	30.49	Sn	2 0 0
31.9194	2.8038	100	0.1378	21.01	Sn	1 0 1
37.8522	2.37688	23.53	0.3149	11.3	Bi	1 0 4
39.5842	2.27678	26.37	0.1968	7.92	Bi	1 1 0
43.749	2.06921	28.94	0.2362	10.43	Sn	2 2 0
44.7339	2.02592	76.1	0.1771	20.56	Bi	2 1 1
45.93	1.97591	3.23	0.09	0.45	Bi	1 1 3
48.59	1.87378	8.41	0.09	1.17	Bi	2 1 1
55.27	1.66209	10.99	0.09	1.53	Sn	3 0 1
62.3824	1.4886	35.73	0.2362	12.87	Sn	1 1 2
64.4833	1.44508	24.96	0.3149	11.99	Sn	3 2 1
70.95	1.32841	5.17	0.09	0.72	Bi	2 1 4
72.21	1.3083	13.58	0.09	1.89	Bi	2 1 4
73.13	1.2941	7.11	0.09	0.99	Sn	4 1 1
79.3262	1.20785	20.79	0.3149	9.99	Sn	3 1 2
81.07	1.18622	2.59	0.09	0.36	Sn	3 1 2
89.2465	1.0966	8.19	0.576	9.72	Sn	3 1 2
95.35	1.04274	7.11	0.09	0.99	Sn	3 3 2

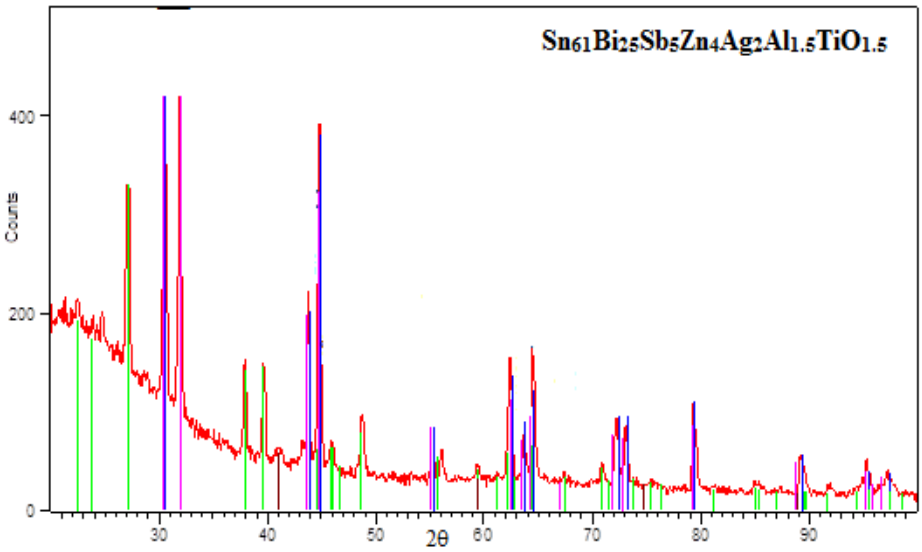

FIG. 1. f) **X-ray diffraction patterns of $Sn_{61}Bi_{25}Sb_5Zn_4Al_{1.5}Ag_2(TiO_2)_{1.5}$ alloy.**

TABLE 1.f) **X-ray diffraction analysis of $Sn_{61}Bi_{25}Sb_5Zn_4Al_{1.5}Ag_2(TiO_2)_{1.5}$ alloy.**

2θ(°)	d(Å)	Intensity (%)	Peak width-FWHM	Area under peak	Phase	h k ℓ
22.41	3.96736	25.92	0.001	0.07	Bi	0 0 3
27.2097	3.27746	53.75	0.2165	46.21	Bi	0 1 2
30.5525	2.92605	100	0.2362	93.79	Sn	2 0 0
31.9576	2.80054	96.23	0.2558	97.77	Sn	1 0 1
37.8925	2.37444	23.19	0.2558	23.56	Bi	1 0 4
39.6494	2.27319	25.81	0.1574	16.14	Bi	1 1 0
40.97	2.20292	3.48	0.09	1.26	Bi	1 1 0
43.8111	2.06643	42.17	0.2165	36.26	Sn	2 2 0
44.8474	2.02106	84.98	0.2952	99.62	Bi	2 1 1
45.9446	1.97531	6.02	0.3149	7.53	Bi	1 1 3
48.7472	1.8681	15.7	0.2362	14.73	Bi	2 1 1
55.2417	1.66287	22.01	0.2165	18.93	Sn	3 0 1
56.007	1.64195	7.73	0.2755	8.46	Sn	3 0 1
59.31	1.55815	3.23	0.09	1.17	Bi	1 0 7
62.3963	1.4883	33.02	0.1574	20.65	Sn	1 1 2
63.6824	1.46131	11.13	0.3149	13.92	Sn	3 2 1
64.4569	1.44561	33.51	0.1968	26.19	Sn	3 2 1
70.927	1.32878	4.82	0.4723	9.04	Bi	2 1 4
72.2376	1.30787	16.59	0.3149	20.74	Bi	2 1 4
73.0425	1.29543	14.66	0.2362	13.75	Sn	4 1 1
79.3238	1.20788	22.12	0.2362	20.75	Sn	3 1 2
89.1731	1.09822	9.43	0.3936	14.75	Sn	3 1 2
91.8905	1.07272	2.66	0.4723	5	Bi	3 1 2
95.4667	1.04177	4.58	0.6298	11.44	Sn	3 3 2
97.237	1.02662	4.64	0.96	23.89	Sn	5 2 1

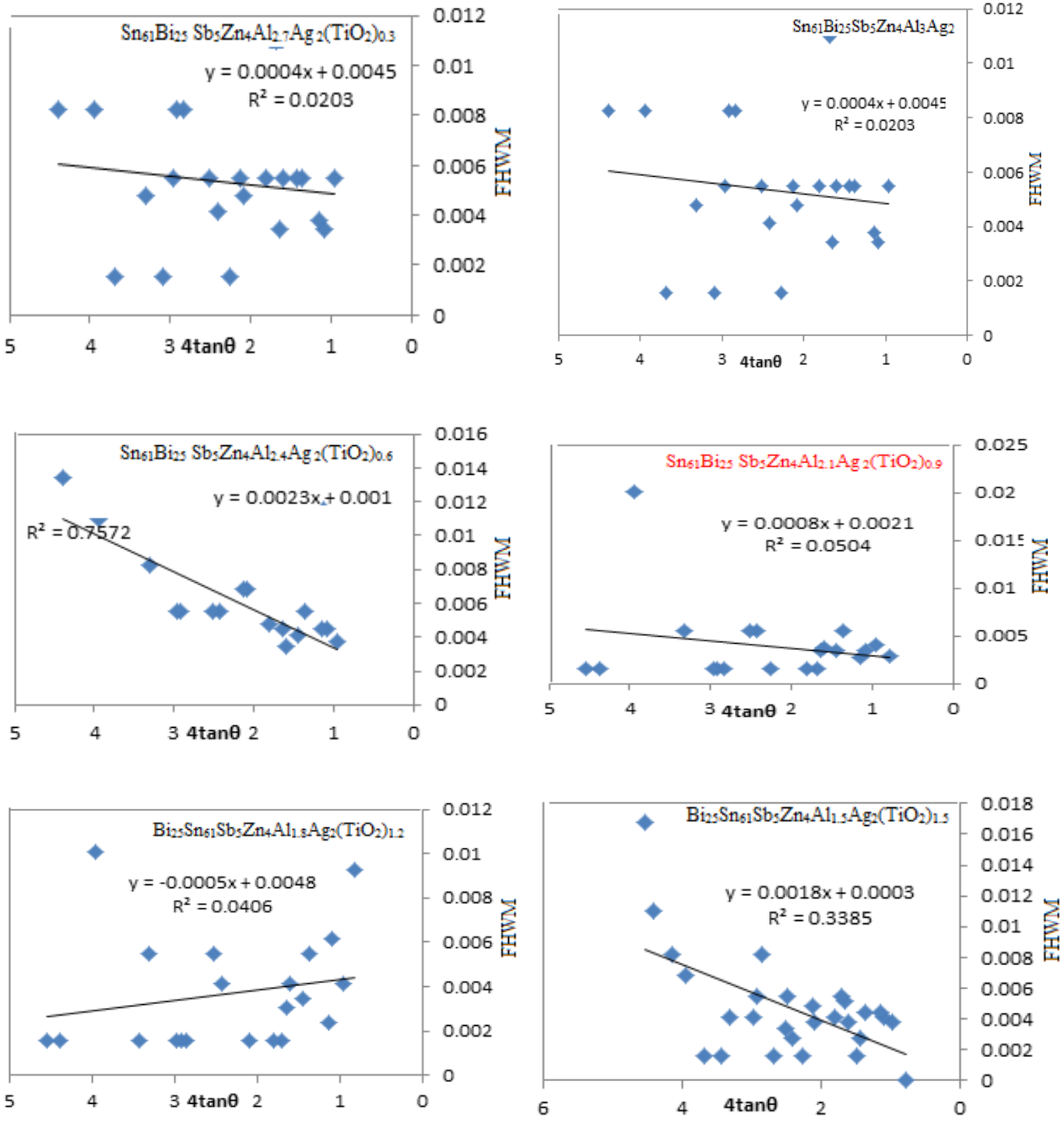

FIG. 1. g) **FWHM versus 4tanθ for $Sn_{61}Bi_{25}Sb_5Zn_4Al_{3-X}Ag_2(TiO_2)_X$ alloys.**

Lattice microstrain of $Sn_{61}Bi_{25}Sb_5Zn4Al_{3-X}Ag_2(TiO_2)_X$ alloys was determined from the relation between FWHM and 4tanθ as shown in FIG. 1g and then presented in TABLE 1g. Lattice microstrain of $Sn_{61}Bi_{25}Sb_5Zn_4Al_3Ag_2$ alloy increased, varied increased, after adding TiO_2 nanoparticles. Estimating crystal size was given by measurement of diffraction pattern broadening. Crystal size of β-Sn in $Sn_{61}Bi_{25}Sb_5Zn_4Al_3Ag_2$ alloy varied after adding TiO_2 nanoparticles as listed in TABLE 1g. $Sn_{61}Bi_{25}Sb_5Zn_4Al_{2.4}Ag_2(TiO_2)_{0.6}$ alloy has higher lattice microstrain and lower β-Sn crystal size.

TABLE 1. g) **Crystal size of Sn and lattice microstrain of $Sn_{61}Bi_{25}Sb_5Zn_4Al_{3-X}Ag_2(TiO_2)_X$ alloys.**

Alloys	(Sn) τ Å^3	ε X10^{-3}
$Sn_{61}Bi_{25}Sb_5Zn_4Al_3Ag_2$	465.93	0.4
$Sn_{61}Bi_{25}\ Sb_5Zn_4Al_{2.7}Ag_{\ 2}(TiO_2)_{0.3}$	522.97	0.4
$Sn_{61}Bi_{25}\ Sb_5Zn_4Al_{2.4}Ag_{\ 2}(TiO_2)_{0.6}$	300.46	2.3
$Sn_{61}Bi_{25}\ Sb_5Zn_4Al_{2.1}Ag_{\ 2}(TiO_2)_{0.9}$	611	0.8
$Bi_{25}Sn_{61}Sb_5Zn_4Al_{1.8}Ag_2(TiO_2)_{1.2}$	692.52	0.5
$Bi_{25}Sn_{61}Sb_5Zn_4Al_{1.5}Ag_2(TiO_2)_{1.5}$	388.4	1.8

Scanning electron micrographs analysis: Scanning electron micrographs (SEM) of $Sn_{61}Bi_{25}Sb_5Zn_4Al_{3-X}Ag_2(TiO_2)_X$ alloys are shown in FIG. 2. SEM of $Sn_{61}Bi_{25}Sb_5Zn_4Al_3Ag_2$ alloy has bismuth grain as spherical bright color, fine bright slab disturbed in tin matrix as black color. SEM of $Sn_{61}Bi_{25}Sb_5Zn_4Al_{2.7}Ag_2(TiO_2)_{0.3}$ alloy has fine bismuth grains with different size and orientation as bright color disturbed in tin matrix as black color.

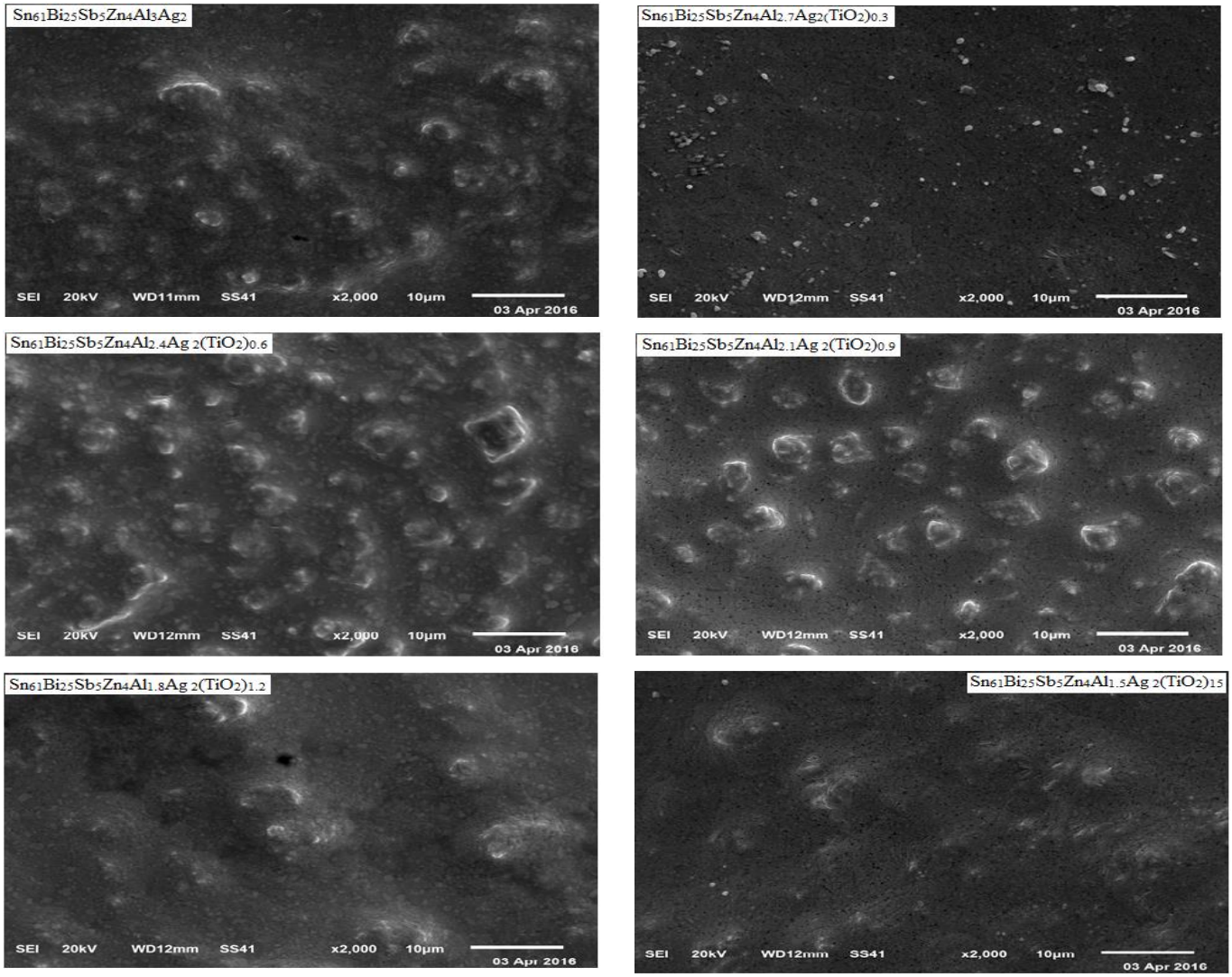

FIG. 2. **SEM of $Sn_{61}Bi_{25}Sb_5Zn_4Al_{3-X}Ag_2(TiO_2)_X$ alloys**

SEM of $Sn_{61}Bi_{25}Sb_5Zn_4Al_{2.4}Ag_2(TiO_2)_{0.6}$ alloy has cluster of bismuth grains with different size, shape and orientation as bright color disturbed in tin matrix as black color. SEM of $Sn_{61}Bi_{25}Sb_5Zn_4Al_{2.1}Ag_2(TiO_2)_{0.9}$ alloy has cluster of bismuth grains with different size, shape and orientation as bright color disturbed in tin matrix as black color. SEM of $Sn_{61}Bi_{25}Sb_5Zn_4Al_{1.8}Ag_2(TiO_2)_{1.2}$ alloy has three dendrite structure, bismuth grains, with different wide as bright color disturbed in tin matrix as black color. SEM of $Sn_{61}Bi_{25}Sb_5Zn_4Al_{1.5}Ag_2(TiO_2)_{1.5}$ alloy has fine grains and dendrite structure of bismuth as bright color disturbed in tin matrix as black color.

Thermal properties: It is very important to study the response of a material to heat. Melting point of solid is a definite temperature which changed it from the solid to the liquid state at a given pressure. The melting point is different for different materials and for each material it slightly varies when the superincumbent pressure varies. However, the alloys have a range of melting and not a fixed melting temperature. But the eutectic alloys have fixed melting point. The melting temperature of a solid material depends on the interatomic and intermolecular bonds. Materials having stronger bonds exhibit higher melting points. The differential scanning calorimetry (DSC) curve (endothermic/exothermic) is used for detecting and characterizing thermal processes qualitatively. FIG. 3 shows differential scanning micrographs of $Sn_{61}Bi_{25}Sb_5Zn_4Al_{3-X}Ag_2(TiO_2)_X$ alloys.

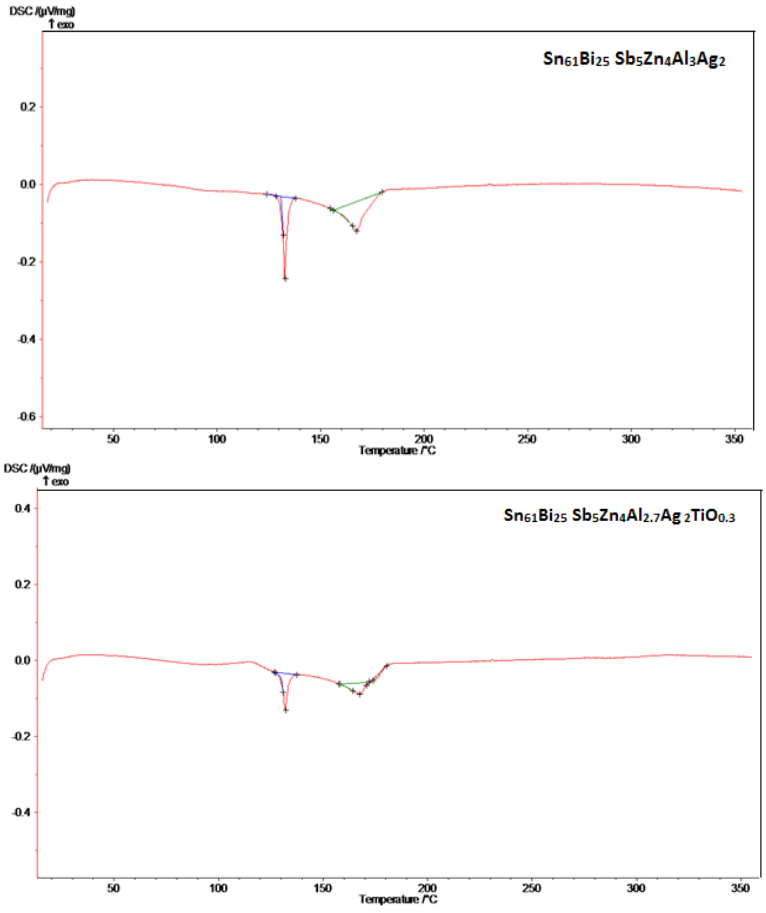

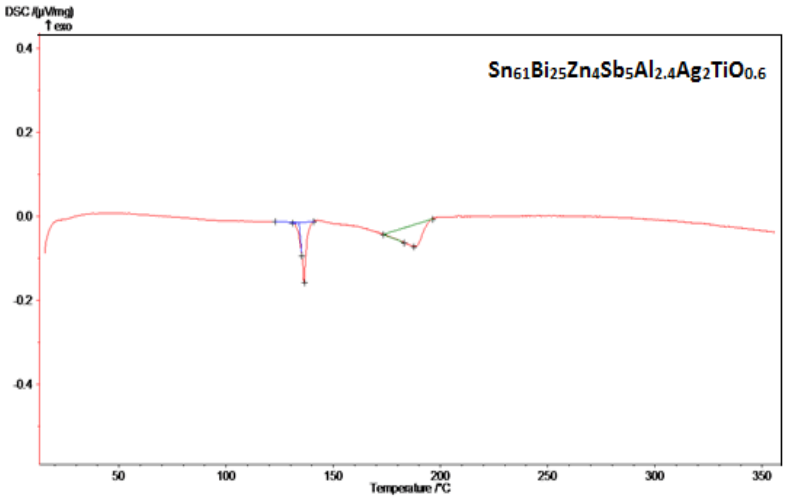
DSC /(µV/mg)
↑ exo
0.4
0.2
0.0
-0.2
-0.4
$Sn_{61}Bi_{25}Zn_4Sb_5Al_{2.4}Ag_2TiO_{0.6}$
50
100
150
200
250
300
350
Temperature /°C

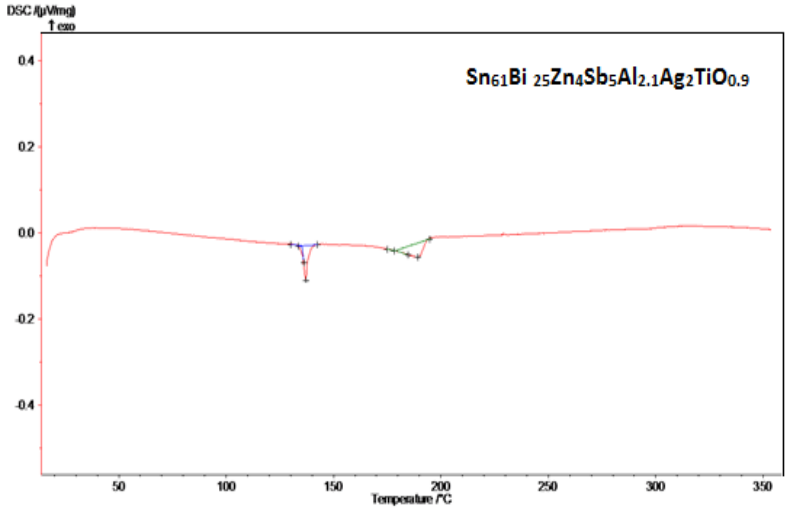
DSC /(µV/mg)
↑ exo
0.4
0.2
0.0
-0.2
-0.4
$Sn_{61}Bi_{25}Zn_4Sb_5Al_{2.1}Ag_2TiO_{0.9}$
50
100
150
200
250
300
350
Temperature /°C

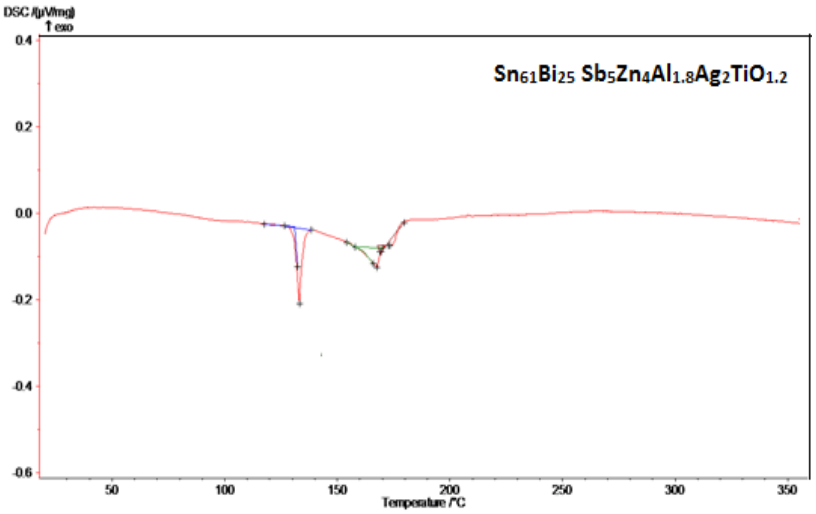
DSC /(µV/mg)
↑ exo
0.4
0.2
0.0
-0.2
-0.4
-0.6
$Sn_{61}Bi_{25}Sb_5Zn_4Al_{1.8}Ag_2TiO_{1.2}$
50
100
150
200
250
300
350
Temperature /°C

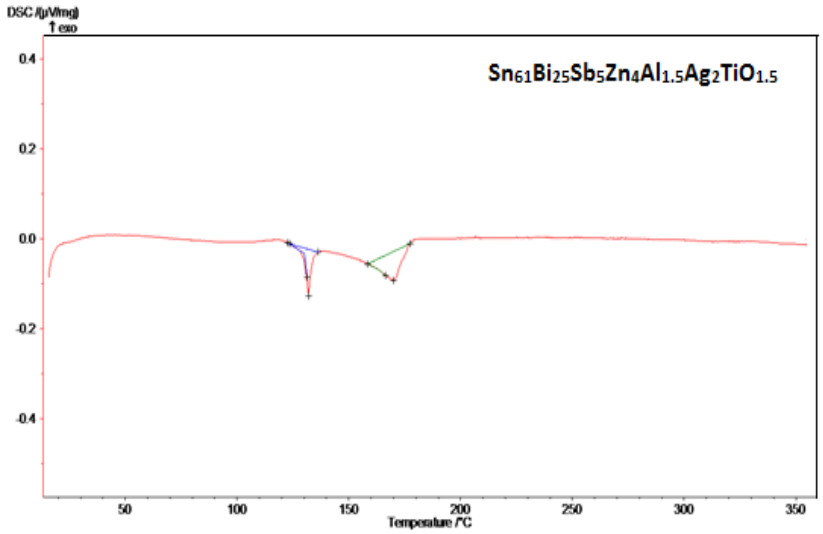

FIG. 3. **DSC graphs of $Sn_{61}Bi_{25}Sb_5Zn_4Al_{3-X}Ag_2(TiO_2)_X$ alloys.**

DSC graphs show the thermal behavior, (endothermic peaks shape, position and intensity), of $Sn_{61}Bi_{25}Sb_5Zn_4Al_3Ag_2$ alloy changed after adding titanium dioxide nanoparticles. Melting temperature (peak one, Tm_1 and peak two, Tm_2) of $Sn_{61}Bi_{25}Sb_5Zn_4Al_3Ag_2$ alloy varied after adding TiO_2 nanoparticles as listed in TABLE 2. It is increased up to 0.9 wt% TiO_2 nanoparticles and then it is decreased, may be due to the structure change. T_1 and T_2 are liquids and solidus temperatures.

TABLE 2. **Defined temperatures of $Sn_{61}Bi_{25}Sb_5Zn_4Al_{3-X}Ag_2(TiO_2)_X$ alloys.**

Alloys	Peak 1	T_{m1}	Peak 2	T_{m2}
$Sn_{61}Bi_{25}Zn_4\ Sb_5\ Al_3\ Ag_2$	T_1=129 T_2=138	133	T_1=159 T_2=180	167.7
$Sn_{61}Bi_{25}\ Sb_5Zn_4Al_{2.7}Ag_2(TiO_2)_{0.3}$	T_1=130 T_2=140	132.1	T_1=160 T_2=180	174.1
$Sn_{61}Bi_{25}\ Sb_5Zn_4Al_{2.4}Ag_2(TiO_2)_{0.6}$	T_1=131 T_2=140	136.6	T_1=175 T_2=200	187.5
$Sn_{61}Bi_{25}\ Sb_5Zn_4Al_{2.1}Ag_2(TiO_2)_{0.9}$	T_1=135 T_2=140	137.7	T_1=180 T_2=195	189.1
$Sn_{61}Bi_{25}\ Sb_5Zn_4Al_{1.8}Ag_2(TiO_2)_{1.2}$	T_1=130 T_2=140	133.3	T_1=160 T_2=180	173.5
$Sn_{61}Bi_{25}\ Sb_5Zn_4Al_{1.5}Ag_2(TiO_2)_{1.5}$	T_1=120 T_2=135	132.1	T_1=158 T_2=177	170.1

Electrochemical corrosion behavior: FIG. 4 shows electrochemical polarization curves for $Sn_{61}Bi_{25}Sb_5Zn_4Al_{3-X}Ag_2(TiO_2)_X$ alloys in 0.25 M HCl. The corrosion potential of the $Sn_{61}Bi_{25}Sb_5Zn4Al_{3-X}Ag_2(TiO_2)_X$ alloys exhibited a negative potential. Also, the cathodic and the anodic polarization curves showed similar corrosion trends. TABLE 3 presents the corrosion potential (E_{Corr}), corrosion current (I_{Corr}), and corrosion rate (C.R) of $Sn_{61}Bi_{25}Sb_5Zn_4Al_{3-X}Ag_2(TiO_2)_X$ alloys. Corrosion rate of $Sn_{61}Bi_{25}Sb_5Zn_4Al_3Ag_2$ alloy varied decreased with increasing the ratio of titanium dioxide nanoparticle. It is because adding titanium dioxide nanoparticle caused heterogeneous microstructure with affected on micro segregation and reactivity of atoms with HCl solution.

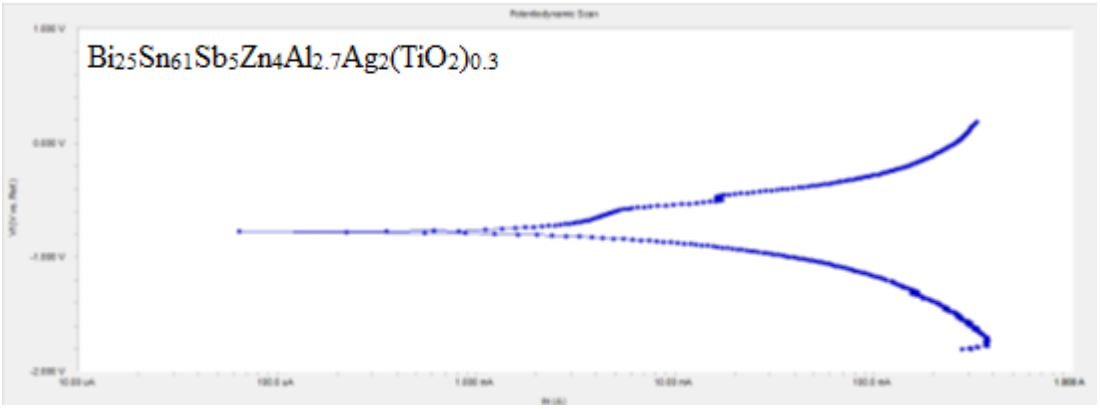
$Bi_{25}Sn_{61}Sb_5Zn_4Al_{2.7}Ag_2(TiO_2)_{0.3}$

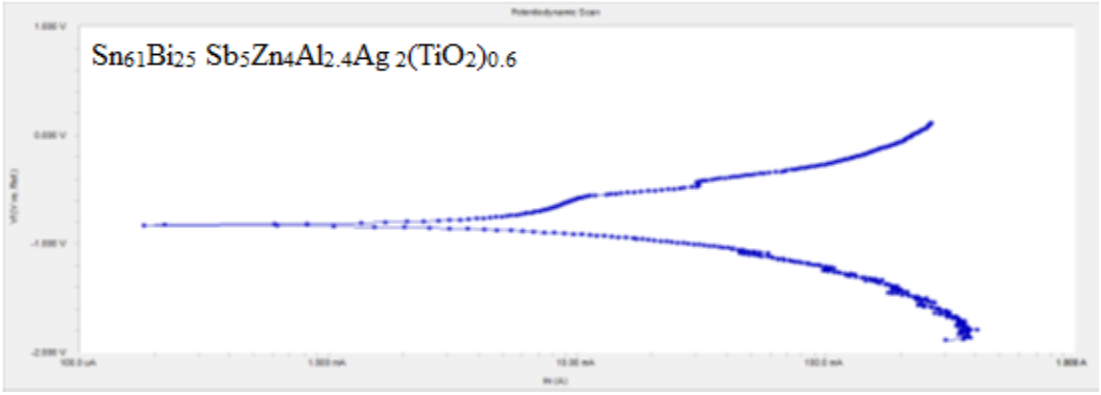
$Sn_{61}Bi_{25}\ Sb_5Zn_4Al_{2.4}Ag_{\ 2}(TiO_2)_{0.6}$

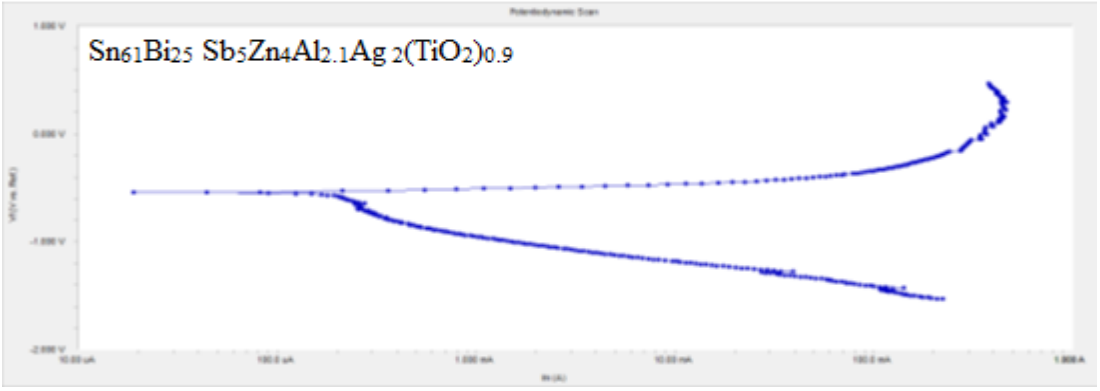
$Sn_{61}Bi_{25}\ Sb_5Zn_4Al_{2.1}Ag_{\ 2}(TiO_2)_{0.9}$

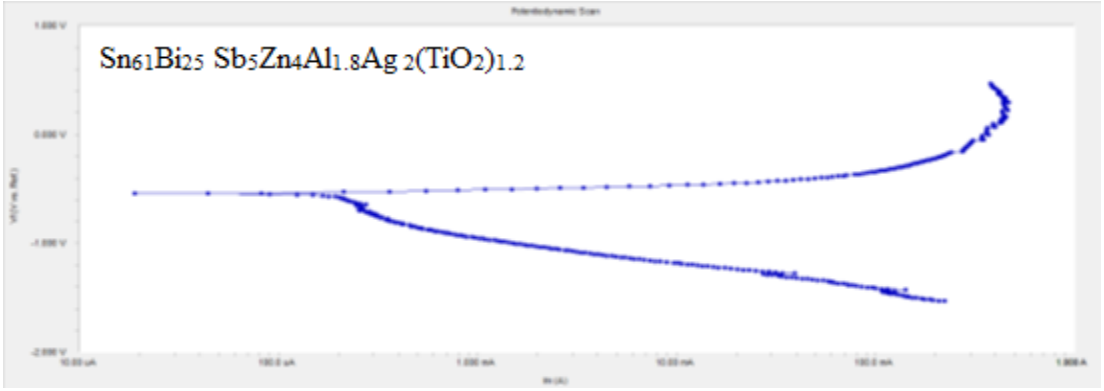
$Sn_{61}Bi_{25}\ Sb_5Zn_4Al_{1.8}Ag_{\ 2}(TiO_2)_{1.2}$

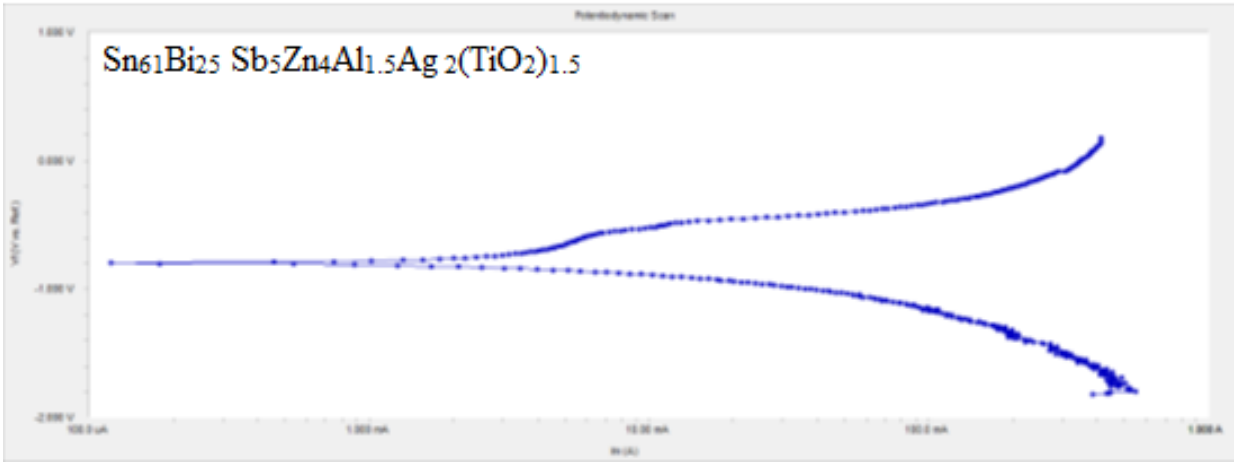

FIG. 4. **Electropolarization curves of $Sn_{61}Bi_{25}Sb_5Zn_4Al_{3-X}Ag_2(TiO_2)_X$ alloys.**

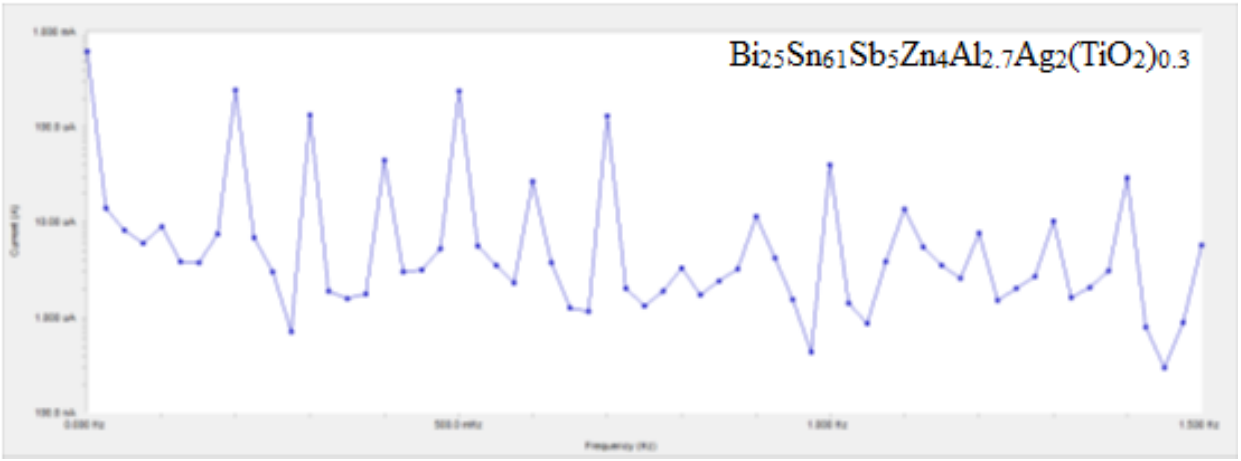

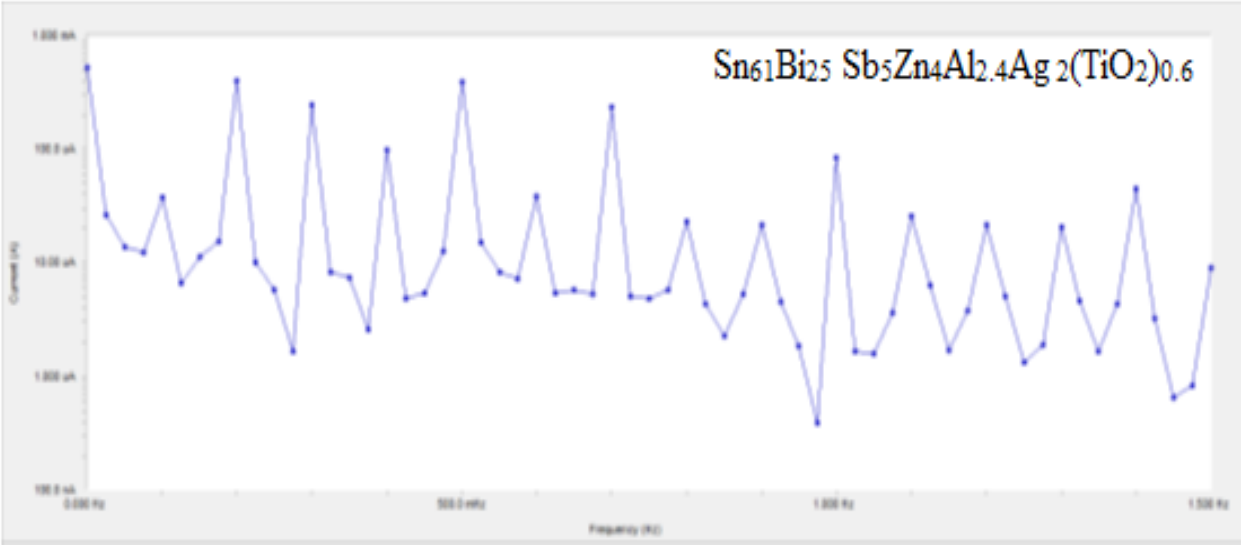

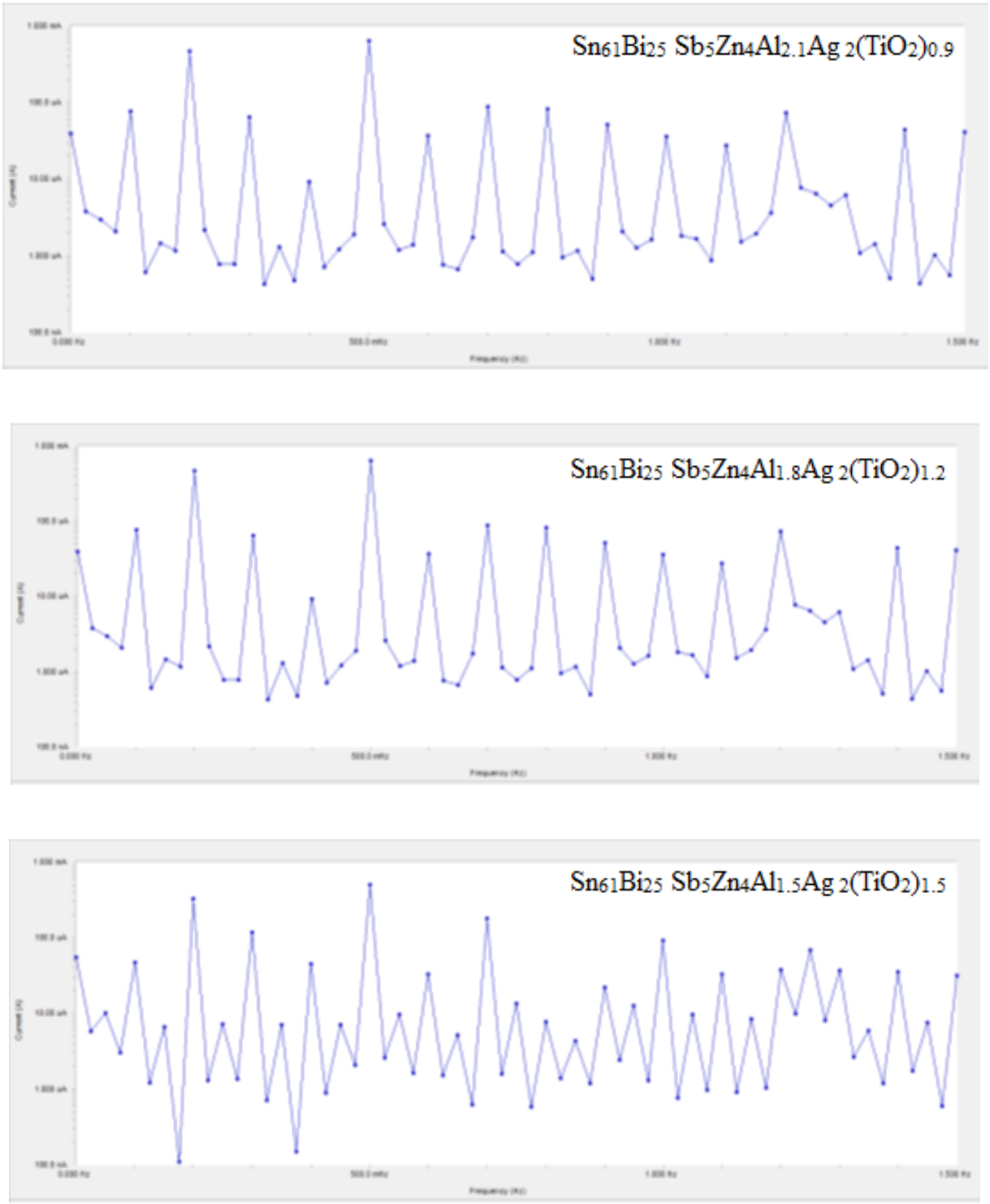

FIG. 5. **Intermodulation spectrum of $Sn_{61}Bi_{25}Sb_5Zn_4Al_{3-X}Ag_2(TiO_2)_X$ alloys.**

The results of EFM experiments are a spectrum of current response as a function of frequency. The intermodulation spectrum of $Sn_{61}Bi_{25}Sb_5Zn_4Al_{3-X}Ag_2(TiO_2)_X$ alloys in 0.25 M HCl solutions are shown in FIG. 5. The larger peaks were used to calculate the corrosion current density and the corrosion rate whish listed in TABLE 4. Corrosion current density and

corrosion rate of $Sn_{61}Bi_{25}Sb_5Zn_4Al_3Ag_2$ alloy varied decreased up to 0.9 wt% titanium dioxide nanoparticle and then increased with increasing the ratio of titanium dioxide nanoparticle. The $Sn_{61}Bi_{25}Sb_5Zn_4Al_{2.1}Ag_2(TiO_2)_{0.9}$ alloy has lower corrosion current density and corrosion rate.

TABLE 3. **Ecorr, Icorr and C. R of $Sn_{61}Bi_{25}Sb_5Zn_4Al_{3-X}Ag_2(TiO_2)_X$ alloys.**

Alloys	E_{corr} µV	I_{corr} µA	C. R mpy
$Sn_{61}Bi_{25}Zn_4\ Sb_5\ Al_3\ Ag_2$	-857.0	156	173
$Sn_{61}Bi_{25}\ Sb_5Zn_4Al_{2.7}Ag_2(TiO_2)_{0.3}$	-776.0	37.9	39.7
$Sn_{61}Bi_{25}\ Sb_5Zn_4Al_{2.4}Ag_2(TiO_2)_{0.6}$	-825.0	81.9	85.8
$Sn_{61}Bi_{25}\ Sb_5Zn_4Al_{2.1}Ag_2(TiO_2)_{0.9}$	-539.0	152	159.1
$Sn_{61}Bi_{25}\ Sb_5Zn_4Al_{1.8}Ag_2(TiO_2)_{1.2}$	-797.0	36	37.7
$Sn_{61}Bi_{25}\ Sb_5Zn_4Al_{1.5}Ag_2(TiO_2)_{1.5}$	-587	63.4	66.35

Table 4. I_{corr} and C. R of $Sn_{61}Bi_{25}Sb_5Zn_4Al_{3-X}Ag_2(TiO_2)_x$ alloys.

Alloys	I_{corr} mA	C. R mpy
$Sn_{61}Bi_{25}Zn_4\ Sb_5\ Al_3\ Ag_2$	566.6	593.3
$Sn_{61}Bi_{25}\ Sb_5Zn_4Al_{2.7}Ag_2(TiO_2)_{0.3}$	222.6	233.1
$Sn_{61}Bi_{25}\ Sb_5Zn_4Al_{2.4}Ag_2(TiO_2)_{0.6}$	323.8	339.0
$Sn_{61}Bi_{25}\ Sb_5Zn_4Al_{2.1}Ag_2(TiO_2)_{0.9}$	199	208.4
$Sn_{61}Bi_{25}\ Sb_5Zn_4Al_{1.8}Ag_2(TiO_2)_{1.2}$	496.6	520.0
$Sn_{61}Bi_{25}\ Sb_5Zn_4Al_{1.5}Ag_2(TiO_2)_{1.5}$	579.8	607.0

Internal friction and thermal diffusivity: Internal friction measurements have been quick fruitful for learning about the behavior of metallic materials. Thermal diffusivity is the measure of heat flowing through the material to the other side. Also, it can be expressed as the rate of change of temperature in a transient heat transfer process. The higher thermal diffusivity of a substance is related to the higher rate of temperature. The thermal diffusivity D_{th} has been derived by Berry and Pritchett [18] from resonance peak. The resonance curves of $Sn_{61}Bi_{25}Sb_5Zn_4Al_{3-X}Ag_2(TiO_2)_X$ alloys are shown in FIG. 6.

TABLE 5. **Internal friction and thermal diffusivity of $Sn_{61}Bi_{25}Sb_5Zn_4Al_{3-X}Ag_2(TiO_2)_X$ alloys.**

Alloys	Q^{-1}	$D_{th} \times 10^{-4}$ Cm^2/sec
$Sn_{61}Bi_{25}Zn_4\ Sb_5\ Al_3\ Ag_2$	0.175	2.586
$Sn_{61}Bi_{25}\ Sb_5Zn_4Al_{2.7}Ag_2(TiO_2)_{0.3}$	0.087	1.377
$Sn_{61}Bi_{25}\ Sb_5Zn_4Al_{2.4}Ag_2(TiO_2)_{0.6}$	0.087	0.77
$Sn_{61}Bi_{25}\ Sb_5Zn_4Al_{2.1}Ag_2(TiO_2)_{0.9}$	0.114	0.615
$Sn_{61}Bi_{25}\ Sb_5Zn_4Al_{1.8}Ag_2TiO_{1.2}$	0.17	7.32
$Sn_{61}Bi_{25}\ Sb_5Zn_4Al_{1.5}Ag_2(TiO_2)_{1.5}$	0.222	15.996

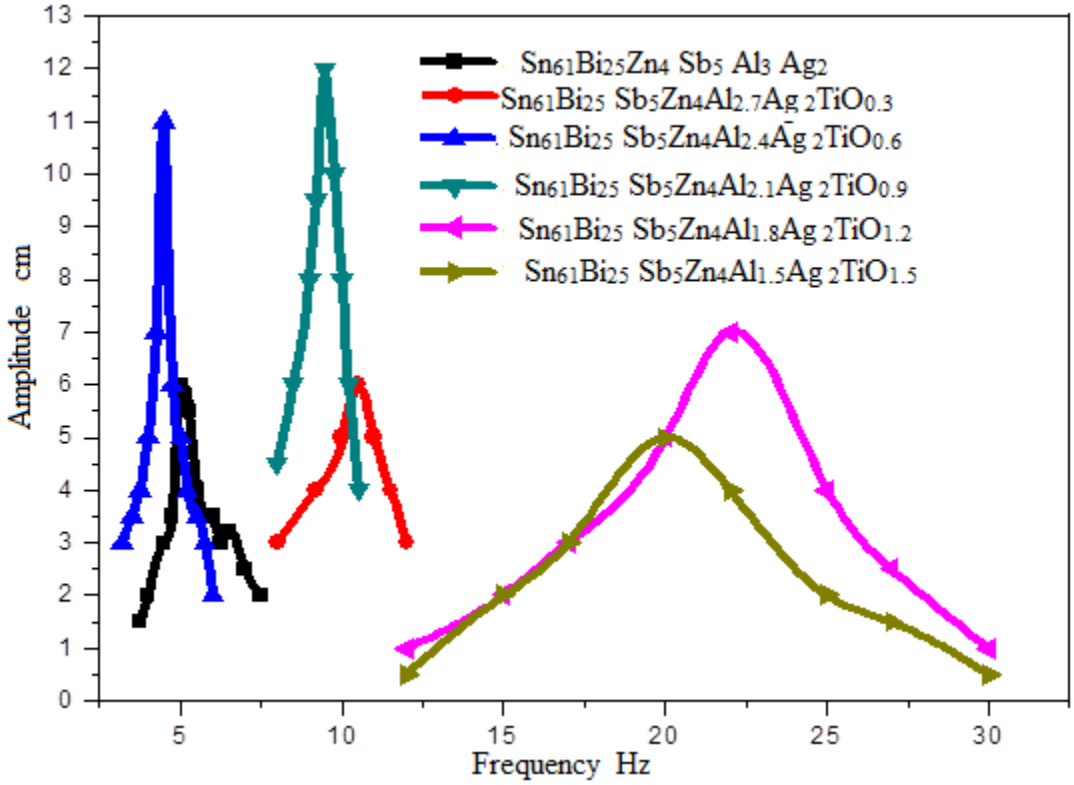

FIG. 6. **Resonance curves of $Sn_{61}Bi_{25}Sb_5Zn_4Al_{3-X}Ag_2(TiO_2)_X$ alloys.**

Calculated internal friction and thermal diffusivity of $Sn_{61}Bi_{25}Sb_5Zn_4Al_{3-X}Ag_2(TiO_2)_X$ alloys are presented in TABLE 5. Internal friction and thermal diffusivity of Sn61Bi25Sb5Zn4Al3Ag2 alloy decreased up to 0.9 wt% titanium dioxide nanoparticle and then increased with increasing the ratio of titanium dioxide nanoparticle as presented in TABLE 5. The $Sn_{61}Bi_{25}Sb_5Zn_4Al_{1.5}Ag_2(TiO_2)_{1.5}$ alloy has higher thermal diffusivity value.

Conclusion

Lattice microstrain of $Sn_{61}Bi_{25}Sb_5Zn_4Al_3Ag_2$ alloy increased after adding TiO_2 nanoparticles. Crystal size of β-Sn phase in $Sn_{61}Bi_{25}Sb_5Zn_4Al_3Ag_2$ alloy varied after adding TiO_2 nanoparticles. Melting temperature of $Sn_{61}Bi_{25}Sb_5Zn_4Al_3Ag_2$ alloy varied after adding TiO_2 nanoparticles. Corrosion rate of $Sn_{61}Bi_{25}Sb_5Zn_4Al_3Ag_2$ alloy decreased with increasing the ratio of titanium dioxide nanoparticle. Corrosion current density of $Sn_{61}Bi_{25}Sb_5Zn_4Al_3Ag_2$ alloy decreased up to 0.9 wt% titanium dioxide nanoparticle and then increased with increasing the ratio of titanium dioxide nanoparticle. The $Sn_{61}Bi_{25}Sb_5Zn_4Al_{2.1}Ag_2(TiO_2)_{0.9}$ alloy has lower corrosion current density and corrosion rate. Internal friction and thermal diffusivity of $Sn_{61}Bi_{25}Sb_5Zn_4Al_3Ag_2$ alloy decreased up to 0.9 wt% titanium dioxide nanoparticle and then increased with increasing the ratio of titanium dioxide nanoparticle. The $Sn_{61}Bi_{25}Sb_5Zn_4Al_{1.5}Ag_2(TiO_2)_{1.5}$ alloy has higher thermal diffusivity value.

REFERENCES

1. El-Bediwi AB, Grayb M, Kamal M. Structure and mechanical properties of modified tin-antimony-lead bearing alloy. Mat Sci Ind J. 2015;13(2):77-84.

2. El-Bediwi AB, Al-Bawee A, Kamal M. Corrosion behavior and physical properties of modified tin-antimony bearing alloy. Mat Sci Ind J. 2015;13(4):136-44.
3. El-Bediwi AB, El-Shafei A, Kamal M. Effect of alloying elements on structure, physical and chemical properties of SnBiZn solder alloy. Mat Sci Ind J. 2015;13(1):1-13.
4. Kamal M, Mazen S, El-Bediwi A, et al. Microstructure, electrical, mechanical and thermal properties of melt-spun bismuth-tin eutectic alloy. Radiat Eff Defect S. 2006;161(2):143-8.
5. Chriašteľová J, Ožvold M. Properties of solders with low melting point. J Alloy Compd. 2008;457(1-2):323-8.
6. Yang CF, Chen FL, Gierlotka W, et al. Thermodynamic properties and phase equilibria of Sn-Bi-Zn ternary alloys. Mater Chem Phys. 2008;112(1):94-103.
7. El-Bediwi AB, Lashin AR, Kamal M. Microstructural evolution and physical properties of lead-tin alloys synthesized by melt-spinning technique. Mat Sci Ind J. 2010;6(2):105-8.
8. El-Bediwi AB, Gouda ES, Kamal M. Effect of bi addition on some physical properties of rapidly solidified Sn-10% Sb solder alloy. Modelling, Measurement and Control. Series C: Chemistry, Geology, Environment and Bioengineering. AMSE. 2004;65(1):1-10.
9. El-Bediwi AB, Lashin AR, Mossa M, et al. Indentation creep and mechanical properties of quaternary Sn–Sb based alloys. Materials Science and Engineering A. 2011;528(10-11):3568-72.
10. El-Bediwi AB. Effects of Cu and Ag as ternary and quaternary additions on some physical properties of SnSb7 bearing alloy. Radiat Eff Defect S. 2004;159(2):125-32.
11. Chen KI, Lin KL. The microstructures and mechanical properties of the Sn-Zn-Ag-Al-Ga solder alloys-the effect of Ag. J Elec Mater. 2002;31(8):861-7.
12. Kamal M, Meikhall MS, El-Bediwi AB, et al. New lead-free solder alloy. Radiat Eff Defect S. 2005;160(7):301-12.
13. Mccormack M, Chen HS, Kammlott GW, et al. Significantly Improved Mechanical Properties of Bi- Sn Solder Alloys by Ag- Doping. J Elec Mater. 1997;26(8):954-8.
14. Cullity BD. The Determination of Crystal Structure. In: Element of x-ray diffraction. Massachusetts: Addison-Wesley Publishing Company, Inc; 1959. p. 297-320.
15. Spinner S, Tefft WE. A method for determining mechanical resonance frequencies and for calculating elastic moduli from these frequencies. In Proc. ASTM. 1961;61:1221-38.
16. Schreiber E, Anderson OL, Soga N. Elastic constants and their measurement. New York: McGraw-Hill; 1974.
17. Timoshenko S and Goodier JN. Theory of elasticity. 2nd Ed. New York: McGraw-Hill; 1951.
18. Berry BS, Pritchet WC. Some physical properties of two amorphous metallic alloys. J Appl Phys. 1973;44(7):3122.